International Journal of Coal Geology 247 (2021) 103851

Contents lists available at ScienceDirect

International Journal of Coal Geology

journal homepage: www.elsevier.com/locate/coal

Particle size and mineralogy distributions in respirable dust samples from 25 US underground coal mines

Emily Sarver *, Çiğdem Keleş, Setareh Ghaychi Afrouz

Department of Mining and Minerals Engineering, Virginia Tech, Blacksburg, VA 24061, USA

ARTICLE INFO

Keywords:
Black lung
Silicosis
Coal mining
Respirable dust
Diesel exhaust
Rock dusting
Thin-seam mining
SEM
Particle characterization

ABSTRACT

Detailed characterization of respirable coal mine dust is critical to understanding occupational health outcomes, as well as improving exposure monitoring and dust controls in mines. However, data on characteristics such as particle size and mineralogy are still scarce, and there are virtually no datasets available that allow direct comparisons across many mines. Following up on a previous effort to characterize dust from eight underground mines in the Appalachian region of the United States, the current study expands the dataset to cover a total of 25 mines across the country. A total of 171 respirable dust samples were collected in standard locations of each mine and analyzed by scanning electron microscopy with energy dispersive X-ray spectroscopy (SEM-EDX). Results demonstrate that significant differences in particle size and mineralogy distributions exist both within and between mines based on sampling location, mine region and/or mining method–and characteristics can be indicative of dust sources. In locations nearby to production or roof bolting, the respirable dust was clearly sourced from the mine strata. Interestingly, in the production location rock-strata sourced dust appeared to be inordinately abundant relative to the actual coal and rock strata heights being mined during sampling. With respect to particle size, diesel particulates and coal dust were generally found to be finer than mineral dust; and mineral dust likely sourced from the rock strata in the mine was finer than that associated with rock dusting products. On average, when considering all particles analyzed between 100 and 10,000 nm, results indicate that about 75% are in the submicron range, however these particles are estimated to account for only about 6% of the mass.

1. Background

A recent study by the National Academies of Science, Engineering and Medicine (2018) reviewed respirable dust sampling and monitoring in coal mines. Among numerous recommendations, the study called for detailed characterization of respirable coal mine dust to shed light on the resurgence of occupational lung disease among miners in the United States—especially in central Appalachia (e.g., see Blackley et al., 2018; Almberg et al., 2018; Reynolds et al., 2018; Hall et al., 2019)—and to support improved strategies for exposure monitoring and disease prevention moving forward.

In response to that recommendation, the authors of the current paper completed a comprehensive analysis of respirable dust samples they had already collected in eight underground coal mines in central and northern Appalachia (Sarver et al., 2019a, 2019b). That work included particle-level analysis of size (0.1–10 μm) and geochemical distributions using scanning electron microscopy with energy dispersive X-ray (SEM-EDX); estimation of mass concentrations of potentially bio-accessible and total acid-soluble metals and trace elements based on digestions of the dust and analysis of the digestates by inductively coupled plasma mass spectrometry (ICPMS); and estimation of mass concentrations of polyaromatic hydrocarbons (PAHs), including 1-nitropyrene (1-NP) which has been considered as a surrogate analyte for diesel exhaust (Scheepers et al., 2003), based on extractions of the dust and analysis of the extracts by high performance liquid chromatography with mass spectrometry (HPLC-MS). Results from the dust digestions and extractions indicated that elemental and PAH concentrations can vary widely between and even within mines. However, the concentrations generally appeared to be low relative to permissible exposure limits (PELs) that could be found for various analytes.

The Sarver et al. (2019a) SEM-EDX results showed variability between and within mines as well, and supported the notion that respirable dust can generally be associated with three primary sources: the coal strata cut at the mine face and crushed by the feeder breaker, which

* Corresponding author.
E-mail address: esarver@vt.edu (E. Sarver).

https://doi.org/10.1016/j.coal.2021.103851
Received 10 June 2021; Received in revised form 25 August 2021; Accepted 15 September 2021
Available online 20 September 2021

is expected to generate mostly coal particles; the rock strata cut and crushed along with the coal or drilled for roof bolting, which is often rich in silica and silicate minerals; and the rock dust products applied to mine surfaces, which are commonly composed of high-purity limestone (dominated by calcium carbonate). In mines operating diesel equipment, the engine emissions represent a fourth major source particles in the respirable range. Moreover, diesel emissions appear to be a more likely source of PAHs than coal dust (Sarver et al., 2019a). Additionally, there might be other minor or intermittent sources of respirable particles including abrasion/wear of various machinery (e.g., cutting or drill bits, conveyor belts, etc.)

Importantly, the Sarver et al. (2019a, 2019b) SEM-EDX results also demonstrated that submicron particles can be abundant in respirable coal mine dust. These include mineral dust such as silica and silicates, which have been identified as likely culprits in the recent resurgence of severe Coal Workers' Pneumoconiosis (e.g., Cohen et al., 2016; Jelic et al., 2017; Hall et al., 2019). Though these finer particles might contribute relatively little to the respirable dust mass, at high number concentrations their increased surface area could have significant implications for exposure response (Oberdörster et al., 2005; Mischler et al., 2016; Riediker et al., 2019; Zhang et al., 2021).

Data on dust constituents and particle sizes is not only critical for informing engineering and administrative controls and monitoring programs in mines, but also the understanding of health outcomes (National Academies, 2018; Abbasi et al., 2021). However, most available data on respirable coal mine dust stems from regulatory compliance sampling efforts, which are practically limited to mass-based measures. In the United States, for example, the regulatory health standards only require measurement of respirable dust concentration (mg/m^3) in the mine environment and the mass percentage of quartz in that dust (30 US Federal Code of Regulations (CFR) part 70, see Code of Federal Regulations, 2021). Several recent studies by other authors have added valuable insights to the larger picture of respirable coal mine dust characteristics by examining samples from one or a small number of mines (e.g., Pan et al., 2021; LaBranche et al., 2021; Trechera et al., 2020; Su et al., 2020). Still, particle-level data are scarce overall—and there are simply no available datasets that allow direct comparisons across a relatively large number of mines.

To fill this gap and expand on the authors' study of the initial eight mines (Sarver et al., 2019a), samples from an additional 17 underground coal mines were collected and analyzed by SEM-EDX. Here, results from all 25 mines are presented and compared.

2. Materials and methods

2.1. Mine details

Table 1 summarizes key details for all 25 mines included in this study. Mines 1–8 are those from which some data have been previously presented (Sarver et al., 2019a, 2019b; Johann-Essex et al., 2017a), and samples from these mines were collected between 2014 and 2015. Samples from Mine 9 were collected in 2013, and samples from Mines 10–25 were collected between 2018 and 2020. The table shows the designated Mine Safety and Health Administration (MSHA) district for each mine at the time of dust sampling. For the purposes of this study, 16 mines were considered to be in the "central Appalachian" region, with mines located in southwestern VA (district 5), southern WV (districts 4 and 12) and eastern KY (district 7). Another nine mines were considered as outside of central Appalachia, including in western PA (district 2), northern WV (district 3), the Illinois coal basin (district 8) or the Western coal basin (district 9).

Table 1 also indicates the primary coal mining method (i.e., by continuous miner or longwall), status of diesel equipment operation, and the predominant roof or floor rock strata being mined along with the coal or drilled for roof bolting during dust sampling. Additionally, the average height of the coal and the rock strata being mined during dust sampling is shown along with the ratio of the rock to total mining height (i.e., a ratio of 0.5 indicates that approximately half of the total mining

Table 1
Summary of key details and samples collected per mine.

Mine No.	MSHADistrict	Prod. method[a]	Diesel status[b]	Roof/floor strata[c]	Average strata height mined			Number of sample sets per location[d]					Total sets
					Coal (m)	Rock (m)	Rock/Total	B	F	I	P	R	
1	4	CM	U	SN	1.2	0.3	0.20	3	1	1	1	1	7
2	4	CM	U	SN	1.1	0.6	0.36	2	1	1	1	1	6
3	4	CM	U	SH/SN	1.4	0.5	0.25	1	1	1	1	1	5
4	4	CM	U	SN	0.9	0.3	0.25	1	1	1	0	1	4
5	2	LW	N	SN/SH/SL	2.1	0.3	0.13	1	3	2	1	3	10
6	3	LW	D	SH	2.0	0.5	0.19	1	3	6	1	4	15
7	12	CM	D	SN/SH/SL	1.7	0.3	0.15	2	3	2	4	3	14
8	12	CM	U	SH	1.3	0.5	0.29	2	3	3	3	4	15
9	5	CM	D	SH	0.6	0.4	0.39	3	4	3	2	2	14
10	7	CM	D	SH/SN	1.1	0.8	0.42	2	2	1	1	1	7
11	5	CM	D	SH	0.8	0.5	0.40	1	1	0	1	1	4
12	5	CM	D	SH/SN	1.3	0.7	0.34	1	0	1	1	1	4
13	5	LW	D	SN/SH	1.6	0.3	0.13	1	1	2	0	2	6
14	5	CM	D	SH	0.8	0.9	0.52	1	1	1	1	0	4
15	4	CM	U	SH	1.0	0.9	0.48	1	1	1	1	1	5
16	3	CM	D	SH	2.1	0.0	0.00	1	1	0	1	1	4
17	3	LW	D	SH	1.6	0.5	0.24	1	0	2	1	2	6
18	3	CM	U	SH	0.8	0.9	0.54	1	1	1	1	1	5
19	8	CM	D	SH/LM	1.9	0.2	0.08	1	1	1	1	2	6
20	8	CM	D	SH/LM	1.8	0.1	0.04	1	2	1	1	1	6
21	12	CM	D	SH/SN	0.9	1.1	0.55	1	1	1	1	1	5
22	12	CM	D	SH	0.8	0.6	0.45	0	1	1	1	0	3
23	9	LW	D	SH	4.3	0.0	0.00	0	0	3	1	1	5
24	9	LW	D	SH/SN	1.8	0.5	0.20	0	1	3	0	2	6
25	12	CM	N	SH/SN	0.2	0.5	0.67	1	1	1	1	1	5
Total sets								*30*	*35*	*40*	*28*	*38*	*171*

[a] Primary production method: CM = continuous miner, LW = longwall.
[b] Diesel status: D = diesel equipment in the mine, N = no diesel equipment in the mine, U = diesel equipment status unknown.
[c] Roof/floor strata being mined/drilled: SN = sandstone, SH = shale, SL = slate, LM = limestone.
[d] Sampling Location: B = bolter, F = feeder, I = intake, P = production, R = return

height was in rock).

2.2. Dust sampling

Respirable dust samples were collected in all mines using the same equipment and procedures described in the earlier study (Sarver et al., 2019a). Briefly, the sampling train consisted of a personal air pump (Escort ELF model; Zefon International, Ocala, FL) that drew mine air through a 10-mm Dorr Oliver nylon cyclone (Zefon International, Ocala, FL) at 2.0 L/min. This is the same cyclone and flow rate used for regulatory compliance sampling of coal mine dust in the United States, which follows a similar approach as most other coal-producing countries; dust sampling procedures have been specifically designed such that the penetration efficiency of particles through the cyclone approximates the accepted respirable convention for lung deposition (ISO, 1995). At 2.0 L/min, the Dorr Oliver cyclone yields about 50% penetration efficiency for 3.5 μm particles (aerodynamic diameter) with a top size of about 10 μm. For all samples included in this study, the dust particles that penetrated the cyclone were deposited onto a 37-mm polycarbonate (PC) filter (track etched with 0.4 μm nominal pore size). The PC filter was housed inside a 2-piece generic polystyrene cassette and backed with a cellulose support pad; all were purchased from Zefon International (Ocala, FL).

In each mine, the goal was to collect samples in five primary locations: in the intake (i.e., clean) airway entering an active section of the mine (I); just downwind from active production by a continuous miner or longwall (P); in the return airway leaving the section (R); adjacent to the feeder breaker or along a main belt (F); and just downwind from an active roof bolter (B). (In longwall mines, the B samples were collected downwind from bolting activities in a development section.) In each location, a sample set was obtained by using multiple sampling trains simultaneously (i.e., to collect replicate filter samples). For this study, just one filter from each set was analyzed, though prior analysis indicated relatively good agreement between replicate filters based on particle distributions (Johann-Essex et al., 2017a).Each sample set was collected over a period of about 2–4 h, which satisfied filter loading requirements (i.e., for SEM-EDX analysis, the filter should not be overloaded) and practical limits on total sampling time in each mine (i.e., usually limited to just one or two shifts or days.)

As shown in Table 1, sample sets could occasionally not be collected in one or two of the targeted locations (i.e., 7 mines × 1 location, 3 mines × 2 locations). On the other hand, sometimes collection of multiple sample sets in a single location was possible (on different shifts or days), in which case results were averaged to yield a single dataset for each unique instance of mine × location. For example, three intake sample sets were collected in Mine 1; thus, results from one PC filter from each set were averaged to yield the Mine 1_Intake results. All told, while a total of 171 filters across all 25 mines were analyzed for this study, the total number of unique mine × location datasets reduces to 112.

2.3. Dust characterization

2.3.1. SEM-EDX analysis

Preparation of the PC filters for analysis by SEM-EDX consisted of cutting a 9-mm subsection of the filter using a stainless steel trephine, and sputter coating by Au/Pd to render the sample conductive. The 9-mm subsection was generally cut off-center to avoid higher dust loading that can occur on the center of the 37-mm filter inside the 2-piece sampling cassettes. Prepared samples were then analyzed using an FEI Quanta 600 FEG environmental scanning electron microscope (ESEM) (Hillsboro, OR, USA) equipped with a backscatter electron detector (BSD) and a Bruker Quantax 400 EDX spectroscope (Ewing, NJ, USA).

To select, size and collect elemental spectra on particles, Bruker's Esprit software (Version 1.9.4) was used to run two computer-controlled routines on each sample. The first routine is for supramicron particles (i.e., with longest dimension between 1000 and 10,000 nm) and it was described in detail by Johann-Essex et al. (2017b) and Sarver et al. (2019a). It was used to analyze about 500 particles in per sample (spread across the filter subsection); on samples with particularly low particle density, sometimes fewer than the targeted 500 particles could be analyzed. The second routine is for submicron particles (100–1000 nm) and a precursor manual version was described by Sarver et al. (2019a). It targeted about 300 particles per sample (again, across the filter subsection). Table 2 summarizes key parameters for both routines. To merge the supra- and submicron data for each sample, particle counts were normalized on a unit-area basis to determine an effective particle density (#/μm^2) in both size ranges.

2.3.2. Particle size and mineralogy distributions

For each particle, the length, width (i.e., perpendicular to length) and projected area were measured by the Esprit software and the dimensions were used to compute a projected area diameter (PAD). The software also used the EDX to capture elemental spectra on each particle, which were reported as normalized atomic % for the following elements per Johann-Essex et al. (2017b): C, O, Al, Si, Ca, Mg, Ti, and Fe. These data were then used to classify each particle (using the criteria shown in Table 3) into one of eight "mineralogy" classes: carbonaceous (C); mixed carbonaceous (MC); aluminosilicates, kaolinite-like (ASK) or other (ASO); other silicates (SLO); silica (S); heavy minerals (M), which mostly included metal sulfides or oxides; or carbonates (CB). (It is acknowledged that particle mineralogy cannot be directly determined using EDX, rather the geochemical data—i.e., atomic % values for analyzed elements—was used to infer likely mineralogy.) Particles that do not fit into one of these classes were classified as "other" (O). The classification criteria were established using respirable-sized particles (sub- and supramicron) generated from high-purity reference materials (see Table S1 in the Supplemental Information).

Using the size and mineralogy classification for each particle, distributions on a number (i.e., count) basis were compiled for each sample. To enable reporting on a mass basis, each particle's dimensions and mineralogy class were also used to estimate its mass. First, the particle volume was estimated as the product of its projected area diameter and short dimension (i.e., the height of the particle as it sits on the filter); the short dimension was determined using a class-specific assumed ratio for the short-to-intermediate (S:I) dimension (i.e., where the intermediate dimension was taken as the particle width). Then, the particle volume was multiplied by an assumed specific gravity (SG) to estimate its mass. The S:I and SG assumptions are given in Table 3 for each mineralogy class. (Note that no such assumptions could be made for the O class, so particles in this class were excluded from mass-based analysis.) Finally, particle masses were summed in each class and divided by the total mass of particles in a given sample to yield mineralogy distributions on a mass % basis.

It is noted that, while the elemental data collection used here was the same as previously described by Sarver et al. (2019a), the mineralogy classification criteria have been updated—primarily to include additional classes. While previous work only used a broad aluminosilicates

Table 2
Summary of key parameters for sub- and supramicron SEM-EDX analysis routines.

Parameters	Submicron	Supramicron
Magnification	10,000×	1000×
Voltage (kV)	10	15
Spot size	5.5	
Working distance (mm)	12.5	
Particle size based on longest dimension (nm)	100–1000	1000-10,000
Frame area (μm^2)	140.25	14,025
Maximum number of frames	80	40
Maximum number of particles per frame	30	50
Total number of particles aimed	300	500

Table 3
Mineralogy classification criteria (updated from Sarver et al., 2019a).

Class	Routine	Normalized Atomic%								Assumptions for mass estimates	
		C	O	Al	Si	Ca	Mg	Ti	Fe	S:I	SG
C	Sub Supra	≥75	<29	≤0.30	≤0.30	≤0.41	≤0.50	≤0.50 ≤0.06	≤0.50 ≤0.15	0.6	1.4
MC	Sub Supra			<0.44 <0.35	<0.44 <0.35	≤1.00 ≤0.50	≤0.50 ≤0.50	≤1.00 ≤0.60	≤1.00 ≤0.60	0.6	1.4
ASK[a]	Sub Supra			≥0.44, (≥37) ≥0.35, (≥39)	≥0.44, (≥42) ≥0.35, (≥32)	(<16) (<8)	(<4) (<15)	(<8) (<13)	(<10) (<13)	0.4	2.6
ASO[a]	Sub Supra			≥0.44, (<37) ≥0.35, (<39)	≥0.44, (<42) ≥0.35, (<32)	(≥16) (≥8)	(≥4) (≥15)	(≥8) (≥13)	(≥10) (≥13)	0.4	2.6
SLO[b]	Sub Supra				≥0.50 ≥0.33					0.4	2.6
S[c]	Sub Supra				≥0.50 ≥0.33					0.7	2.7
M	Sub Supra			>1.00				>1.00	>1.00	0.7	5.0
CB	Sub Supra	<88	>9			>1.00 >0.50	>0.50			0.7	2.7

[a] To differentiate ASK from ASO, additional limits for Al, Si, Mg, Ca, Ti and Fe are shown in parenthesis (normalized to exclude C and O).
[b] Additional limits for SLO: Si/(Al + Si + Mg + Ca + Ti + Fe) < 0.5.
[c] Additional limits for S: Al/Si < 1/3 and Si/(Al + Si + Mg + Ca + Ti + Fe) ≥ 0.5.

(AS) class, that class has now been split into ASK and ASO. The ASK class may be of interest for comparison to other measures of kaolinite. For instance, MSHA Method P7 (2008) is used for compliance monitoring of quartz in respirable coal mine dust; since kaolinite presents an interference for the P7 quartz mass measurement by Fourier Transform Infrared (FTIR) spectroscopy, the kaolinite mass is also determined to enable the quartz correction. Also, the SLO class has been added here. Particles in this class would have previously been binned as "other".

2.3.3. Evaluation of diesel particulates

As discussed by Sarver et al. (2019a, 2019b), the C class is expected to be dominated by coal dust particles in the supramicron range, however diesel particulates may also be present in the submicron range. This can confound interpretation of particle sources in the mine dust samples.

In the current work, an effort was made to evaluate the presence of diesel particulate matter (DPM) in all 171 mine dust samples. This was done by visually inspecting SEM images from each sample that were gathered during the submicron SEM-EDX routine (at 10,000× magnification). Images were scanned by a single user to determine whether DPM could be visually confirmed by its characteristic morphology (chains or clusters of ultrafine carbonaceous particles), and each sample was binned into one of three categories: particles observed that are consistent with DPM appearance (DPM); no particles observed that are consistent with DPM appearance (no DPM); or particles observed which *might* be DPM (maybe DPM). Fig. 1 shows representative images for each category.

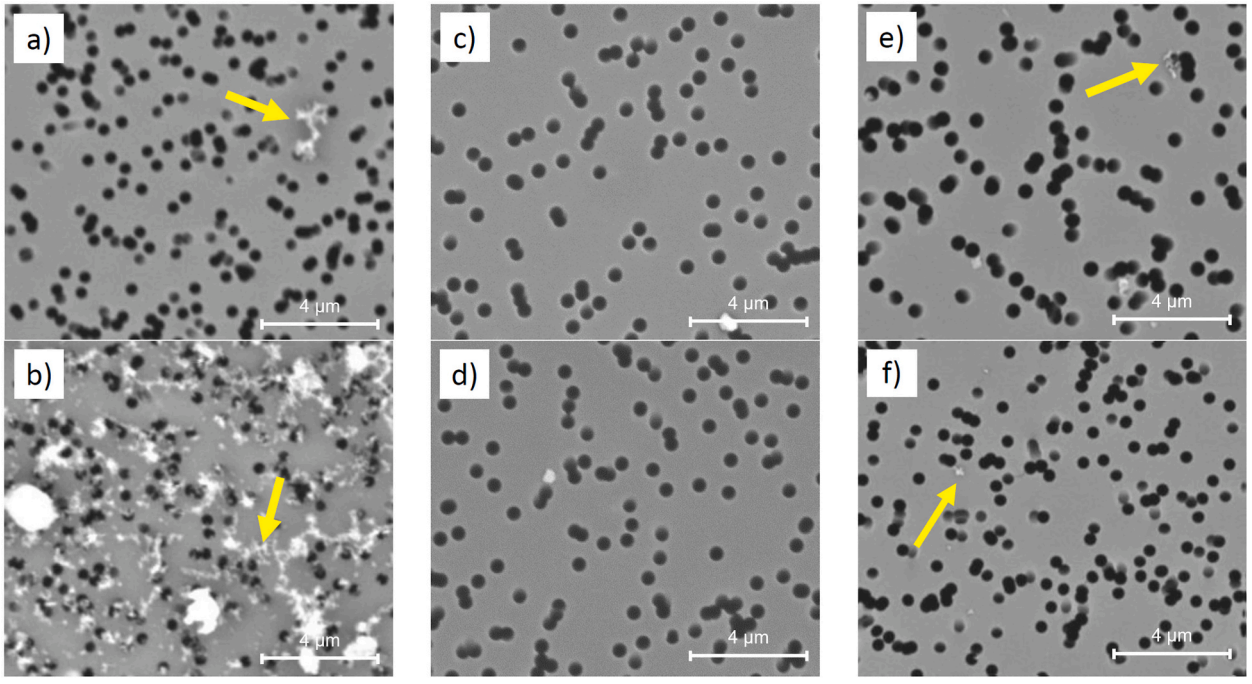

Fig. 1. Representative SEM images from respirable dust samples collected in intake airways. Images a) and b) show particles that are clearly consistent with DPM morphology (note there are many such particles in image b); images c) and d) show no particles consistent with DPM morphology; and images e) and f) show particles that might be DPM. (Note the black circles are the pores in the PC filter).

2.4. Statistical analysis

The mine dust samples were grouped to support testing for statistically significant differences in particle size and/or mineralogy based on the following independent variables: presence of diesel particulates (DPM, no DPM), sampling location (B, F, I, P, R), mine region (central Appalachia, outside of central Appalachia), and mining method (continuous miner, longwall). Comparisons between group means were conducted using one-way analysis variance (ANOVA), with null hypothesis defined as statistically equal means and significance level $\alpha = 0.05$. In cases where data was determined to have a non-normal distribution (based on the Q-Q plot of residuals), it was transformed using the cube root. For most comparisons (i.e., presence of DPM, mine region, mining method), analysis was done using only two sample groups so probability values (p) < 0.05 indicate significant difference between those group means. However, for comparisons between sampling locations, there were five groups. In this case, when ANOVA testing yielded $p < 0.05$, the Tukey-Kramer Honestly Significant Difference (HSD) test was used to identify pairs with significantly different means.

Exploratory factor analysis was also used to look for correlations between the relative abundance of particles in the different mineralogy classes. For this, the principal axis and Varimax rotation methods were used.

All statistical analysis was conducted with JMP ® Pro, Version 15.0.0.0. (SAS Institute Inc., Cary, NC).

3. Results and discussion

The SEM-EDX results for samples from all mines are summarized in the Supplemental Information. Table S2 shows mineralogy distributions (number %) for the entire size range of particles analyzed, and Table S3 shows the distributions following application of a 400-nm lower size threshold to minimize the influence of DPM on the results (see below).

3.1. Influence of diesel particulates on dust analysis

As mentioned, the presence of DPM in some mine dust samples might confound analysis of dust, particularly fine particles in the C class that may be sourced from coal strata. To explore, results of the visual inspection for DPM in the SEM images were used. Images were inspected for all 171 mine dust samples: 68 were observed to have DPM (and all of these were from mines listed as operating or possibly operating diesel equipment in Table 1), 67 were observed to have no DPM, and 28 were placed in the "maybe DPM" category. (No C particles were found in the remaining eight samples, so they were excluded from the following analysis.)

The effect of DPM on the C particle size distribution (number %) was examined by incrementally applying a lower size limit on the particles included in the distribution (i.e., from no limit, up to 600 nm PAD). With no limit, all C particles captured by the SEM-EDX analysis are included the distribution; with a 600-nm limit, C particles with PAD <600 nm are excluded from the distribution. In essence, this exercise was aimed at establishing a threshold size below which DPM affects the distribution of particles in the C class, and above which it does not. Fig. 2 shows the average cumulative size distribution of C particles for the DPM and no DPM sample groups using six different size bins as the lower limit. The data clearly show that, when all particles are considered (i.e., no limit), samples with DPM have a finer distribution of C particles than those without DPM. However, as the lower size limit is increased, the DPM and no DPM group distributions begin to converge—and become very similar for the 400-nm limit. This is the same threshold that was used in the previous study of dust samples from Mines 1–8 (Sarver et al., 2019a) and is in reasonable agreement with data from Birch and Noll (2004), which indicated a maximal separation of DPM and coal dust between about 500–700 nm in mines operating diesel equipment.

ANOVA was performed to evaluate the 400-nm threshold using the D_{50} values for C particles in each sample. (The D_{50} is a measure of particle size distribution, defined as the size at which 50% of particles are finer than the D_{50} size.) Results confirmed that the DPM sample group has significantly finer C particles than the no DPM group if a lower limit is not placed on particle size; but there is no significant difference in the group means after the 400-nm threshold is applied (Table 4). (Notably, the same conclusion is reached by applying a 500-nm or 600-nm threshold, however increasing the threshold ultimately results in exclusion of more particles from subsequent analysis.) These results support using the 400-nm threshold to minimize influence of DPM on analysis of dust constituents. Moreover, this threshold also eliminates any concern that dust analysis is biased due to particle losses through the pores in the PC filters (nominally 0.4 μm and measured at about 300–400 nm by SEM).

3.2. Particle size distributions on the basis of number

To gain insights to overall trends in the dust particle size as a function of mineralogy, Fig. 3 shows average size distributions (number %) across all 25 mines included in the dataset. To evaluate the relative sizes of coal

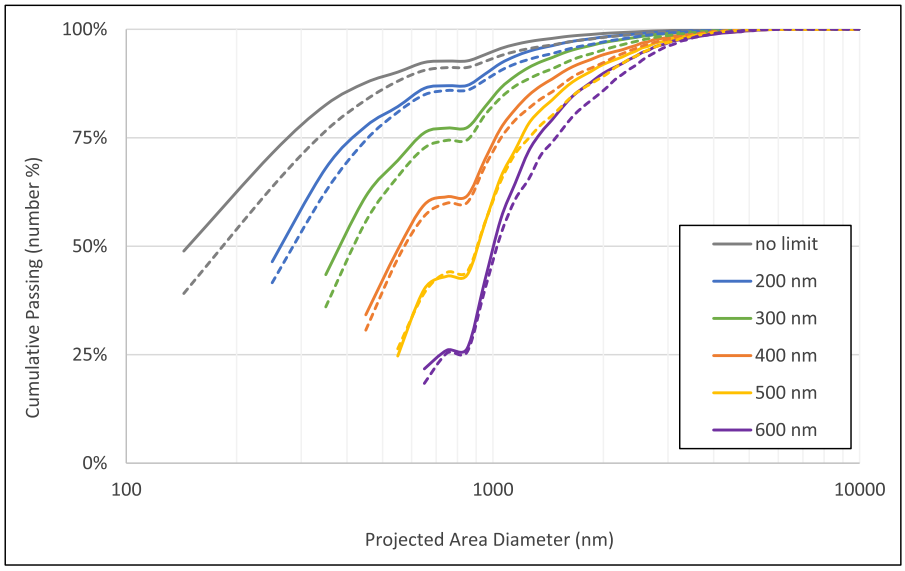

Fig. 2. Average cumulative C particle size distributions (number %) for samples with DPM (solid lines) and with no DPM (dashed lines) using lower size limits between 100 and 600 nm. Data was computed using number percentage of C particles in 100-nm wide size bins, with points plotted at the bin mid-size (e.g., 250 nm for the 200–300 nm bin); for the smallest bin, the width is 87–200 nm and the bin mid-size is 144 nm. The characteristic shift in each curve around 850 nm is an artifact of merging data from the sub- and supramicron SEM routines.

Table 4
Summary of statistics for comparison of C particle D_{50} values (number basis) between DPM and no DPM sample groups. Shaded *p*-value indicates significant difference.

	No lower size limit		400-nm lower size limit	
	DPM	No DPM	DPM	No DPM
n-value	68	67	67	61
Lower 95% CI (nm)	135	190	567	588
Mean D_{50} (nm)	154	211	641	659
Upper 95% CI (nm)	173	233	717	730
p-value	0.0001		0.7486	

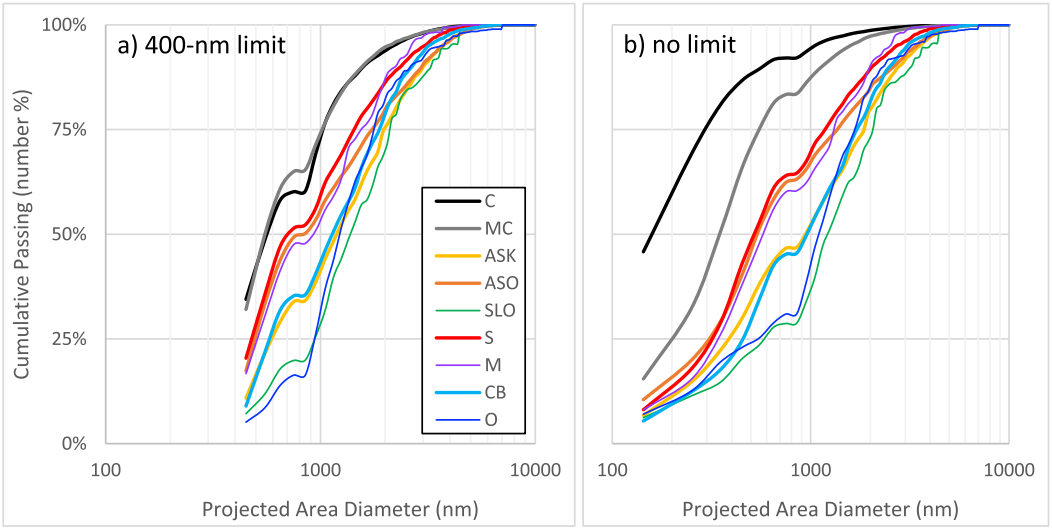

Fig. 3. Average cumulative particle size distributions (number %) across all mines and sampling locations by mineralogy class (C = carbonaceous, MC = mixed carbonaceous, ASK = kaolinite-like aluminosilicates, ASO = other aluminosilicates, SLO = other silicates, S = silica, M = heavy minerals, CB = carbonates, O = other). Results are shown a) with and b) without the 400-nm threshold established to minimize the influence of DPM on the C class. Since the number of samples from each location varied by mine, sample results were first averaged by location in each mine and then by mine, yielding $n = 112$ as explained in section 2.2. Data were computed using number percentage of particles in 100-nm wide size bins, with points plotted at the bin mid-size.

and mineral dust, Fig. 3a shows the distributions using the 400-nm threshold to exclude finer particles from the analysis. The C and MC classes, which trend together and are expected to include mostly coal dust, exhibit finer distributions than any of the mineral classes. Considering only the ≥400 nm particles, about 75% of C and MC particles have PAD less than 1000 nm, and 33% have PAD less than 500 nm. From Fig. 3b (no limit on particle size), the MC class, which is not expected to be substantially influenced by DPM, can be evaluated across the entire size range analyzed by the SEM-EDX. Inclusion of particles <400 nm in the MC distribution indicates that nearly 90% of the particles are less than 1000 nm and 67% are less than 500 nm.

In Fig. 3, the mineral particles appear to form three main groups: S, ASO and M, which are relatively fine; CB and ASK, which are coarser; and SLO and O, which are coarsest. These groupings might be related to dust generation mechanisms and/or physical properties of the minerals themselves. Across the entire size range analyzed by the SEM-EDX, about 67% of S, ASO and M particles, 52% of CB and ASK particles, and 40% of SLO and O particles have a PAD less than 1000 nm (Fig. 3b). For the same groups, respectively, about 45%, 32% and 23% of particles have a PAD less than 500 nm. This is consistent with the earlier findings for Mines 1–8 that showed substantial fractions of dust particles in the submicron size range (Sarver et al., 2019a). Moreover, it is consistent with recent findings by Pan et al. (2021), who reported relatively high abundance of both rock (mineral) and coal particles in the submicron range for respirable dust samples collected in an underground coal mine.

Fig. 4 compares the size distributions for particles in each major mineralogy class by sampling location, and the data are also separated by mine region (i.e., in or outside of central Appalachia). It is noted that the SLO, M and O classes generally had very low abundances of particles across the entire sample set and are therefore not included in Fig. 4.

Overall, dust in samples from the P, R and B locations is relatively finer than in the I and F locations. This makes sense given the proximity of the P, R and B locations to key dust-generating activities, and it is consistent with previous findings for dust from only Mines 1–8 (Sarver et al., 2019a). The trend is especially apparent for particle classes expected to be primarily associated with mining or drilling in rock strata (i.e., ASK, ASO and S) and can be observed for both regions.

Particles in the MC class are also somewhat finer in the samples from the P, R and B (versus I and F) locations in the central Appalachian mines and the R samples from the other mines. However, the C class distributions do not exhibit such differences with respect to sampling location. This may be an artifact of DPM continuing to have some influence in certain samples, especially those with relatively few coal dust particles (e.g., I samples in central Appalachia).

CB particles, which are expected to be primarily sourced from application of rock dusting products (frequently high-quality limestone, Barone et al., 2016), are markedly coarser in the central Appalachian samples than those from other mines. This may be due to differences in the rock dust products being used regionally. It is also possible that some CB dust is generated from the rock strata in some mines (e.g., the roof strata in Mines 19 and 20 included limestone), which may explain the relatively finer CB particles in P and/or R locations in the mines outside of central Appalachia.

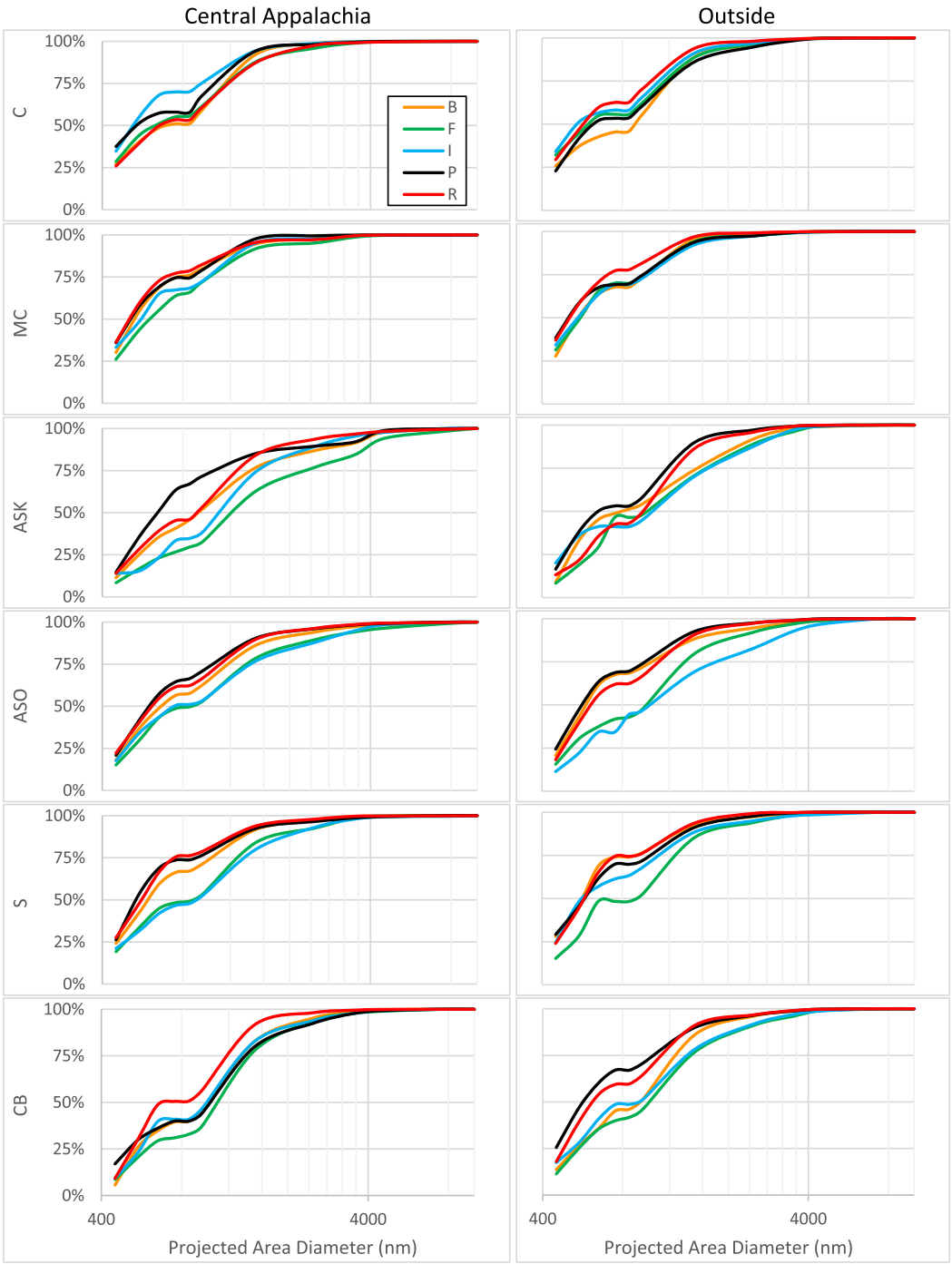

Fig. 4. Average cumulative particle size distributions (number %) for each major mineralogy class by sampling location, with results separated by mine region. (C = carbonaceous, MC = mixed carbonaceous, ASK = kaolinite-like aluminosilicates, ASO = other aluminosilicates, SLO = other silicates, S = silica, M = heavy minerals, CB = carbonates, O = other; B = roof bolter, F = feeder breaker, I = intake, P = production, R = return). Results are shown with the 400-nm threshold established to minimize the influence of DPM on the C class. Since the number of samples from each location varied by mine, sample results were first averaged by location in each mine and then across the mine region, yielding $n = 15$ for B, F, and I, and $n = 14$ for P and R locations in central Appalachia; and $n = 7$ for B and F, $n = 8$ for I and P, and $n = 9$ for R in mines outside central Appalachia. Data were computed using number percentage of particles in 100-nm wide size bins, with points plotted at the bin mid-size.

3.3. Mineralogy distributions on the basis of number

To explore correlations between the abundance (number %) of dust particles in each mineralogy class, factor analysis was performed on all 171 samples following application of the ≥400 nm threshold to minimize influence of DPM. Four factors were found to explain 71% of the total variance, with the first two explaining roughly 20% each and the second two explaining roughly 15% each (Table 5).

Factor 1 appears to be associated with rock-strata sourced dust. It shows strong positive correlation between ASK and ASO abundances, which are negatively correlated with C and CB. The negative correlations are likely an artifact of rock-strata sourced dust dominance in some samples, at the exclusion of dust from other sources such as the coal strata or rock dusting products.

Table 5
Results of exploratory factor analysis considering the abundance of particles (number %) in each mineralogy class (C = carbonaceous, MC = mixed carbonaceous, ASK = kaolinite-like aluminosilicates, ASO = other aluminosilicates, SLO = other silicates, S = silica, M = heavy minerals, CB = carbonates, O = other). For this analysis, abundances were determined after applying a 400-nm lower size limit to the particle data in each sample. Explained variance is indicated for each of the four factors, and shading intensity indicates relative direction and strength of variable correlations.

Class	Factor 1 (20.5%)	Factor 2 (20.0%)	Factor 3 (16.4%)	Factor 4 (13.9%)
ASO	0.85	-0.10	-0.12	0.19
ASK	0.64	-0.24	0.21	-0.22
SLO	-0.08	0.85	0.09	0.13
O	0.04	0.80	-0.08	-0.12
CB	-0.33	0.37	-0.47	-0.51
MC	-0.08	-0.19	0.80	0.03
M	0.00	0.25	0.72	-0.12
C	-0.78	-0.36	0.12	-0.13
S	0.04	0.06	-0.11	0.92

Factor 2 exhibits strong positive correlation between SLO and O abundance, which are generally very low (i.e., O is <3% in all but 9 samples; SLO is <3% in all but 1 sample). The moderately positive correlation between these constituents and CB, however, indicates that this factor is probably associated with specific rock dusting products or samples with sufficient rock dust product contribution that that the minor product constituents (i.e., SLO and O) are detectable in the sample. Factor 2 also shows a moderately negative correlation between abundance of C and that of SLO, O and CB. This is probably another artifact of a dominant dust source in some samples; when the contribution from rock dusting products is very high, it is so at the exclusion of other dust sources (e.g., coal or rock strata).

Factor 3 is most likely related to coal dust. It shows high positive correlations between MC and M abundances. MC particles are expected to be primarily coal dust with minor impurities. M particles, though generally low in abundance, often include metal sulfides (e.g., pyrite) that may be associated with the coal seam. Interestingly, MC and C only exhibit a weakly positive correlation within this factor. This might be related to residual influence of DPM in some samples without many other particles. Moreover, while the sum of C and MC abundances can be loosely interpreted as the coal dust component of a sample, the split of particles between these two classes varies considerably. Factor 3 also shows a moderately negative correlation between CB and the MC and M, again illustrating the fact that some samples are dominated by dust from certain sources.

Factor 4 shows a negative correlation between S and CB. This suggests that silica particles in the mine dust samples are generally not sourced from rock dusting products—although S abundance is not strongly correlated with abundance of other rock strata sourced minerals (e.g., ASO) either. This might be because rock strata sourced dust is ubiquitous across the sample set, whereas S particles are clearly more abundant in the samples from some mines versus others (e.g., see Table S3).

Notably, while the factor analysis does help explain variance in the dust constituents with respect to expected sources, the findings do not indicate that the groupings of mineral classes seen in Fig. 3 are necessarily due to common sources. For example, none of the factors revealed strong correlations between ASK and CB, nor between ASO, S and M. This lends some credence to the interpretation that mineral dust size is related to properties of the mineral itself rather than the source material.

To further explore the mineralogy distributions, the following sections present data by sampling location, mine region and mining method.

3.3.1. *Effect of sampling location*

Fig. 5 shows the relative abundance of particles (number %) in each mineralogy class across all 25 mines, with the data separated by sampling location. (It should be noted that these data cannot be used to assess the relative concentration of dust in each sampling location, only the distribution of the particles analyzed.) Distributions are shown for particles <400 nm, ≥400 nm, and for the entire size range analyzed ("total").

The general trends for all 25 mines are fairly similar to those previously reported for just Mines 1–8 (Sarver et al., 2019a), although the improved submicron SEM-EDX routine used here indicates relatively higher C content in the finer size range. For many samples, this is largely related to the presence of DPM, especially in the <400 nm range (Fig. 5a). DPM was observed most frequently in intake (I) samples (23 of 40) and feeder (F) samples (15 of 35). However, even after applying the 400-nm threshold to minimize influence of DPM on the mineralogy results (Fig. 5b), the I and F samples generally have more C particles and fewer mineral dust particles than samples from other locations. The prevalence of CB particles, as opposed to other minerals, in I samples is indicative of rock dusting activities rather than drilling or mining rock strata.

Bolter (B), production (P) and return (R) samples are sometimes also influenced by DPM, which was observed in 10 of 30 B samples, 8 of 28 P samples, and 12 of 38 R samples. However, samples from these locations have relatively more (and finer) mineral dust, especially in the AS (ASO + ASK) and S classes, which is likely sourced from drilling or mining rock strata. Moreover, based on C and MC abundances shown for particles ≥400 nm, samples from these locations appear to have relatively low coal content. This is expected in the B samples since most of these were collected upwind of production activities, but it is less intuitive for the P and R samples which were collected downwind of coal production.

Indeed, six P samples showed exceedingly low C + MC content (i.e., ≤2% of the particle counts after applying the 400-nm threshold). The samples were from Mines 10, 11, 14, 20, 21 and 22, all of which are in central Appalachia except Mine 20; the R samples from Mines 11 and 21 also showed C + MC ≤2%. These results might be influenced by several factors, including the possibility that coal dust particles could be misclassified by the SEM-EDX in some cases. (Since the C and MC classification criteria, see Table S1, are set to essentially rule out particles based on their Al, Si, Ca, Mg, Fe and Ti elemental response, misclassification of coal could happen if mineral particles are in very close proximity to the coal during analysis, or if the coal itself has some mineral impurity. Misclassification of other particle types is less likely since criteria for the mineral classes are set to include particles with sufficient elemental response.) That said, previous work on respirable dust in several central Appalachian mines has also shown very low coal (and high *non-carbonate* minerals) mass content using thermogravimetric analysis–especially in samples collected near production activities (Phillips et al., 2017, 2018). Thus, while it is acknowledged the SEM-EDX results might somewhat underestimate coal content in some of the samples included in the current study, the general trends presented here are consistent with other work using different analytical methods. Other factors influencing relatively low coal content (and high rock-strata sourced dust content) in P and R samples could include properties of the dust generating materials themselves (e.g., some rock strata may be more likely than coal strata to generate dust in the respirable range) or differential efficiencies of various dust controls (e.g., water sprays may work better to control respirable coal dust as opposed to mineral dust).

To identify statistically significant differences between the abundance (number %) of dust (≥400 nm) in each mineralogy class across the various sampling locations, ANOVA and Tukey-Kramer HSD tests were performed. Table 6 presents the results, which basically compare the data shown in Fig. 5b. (Note that the six P samples mentioned above

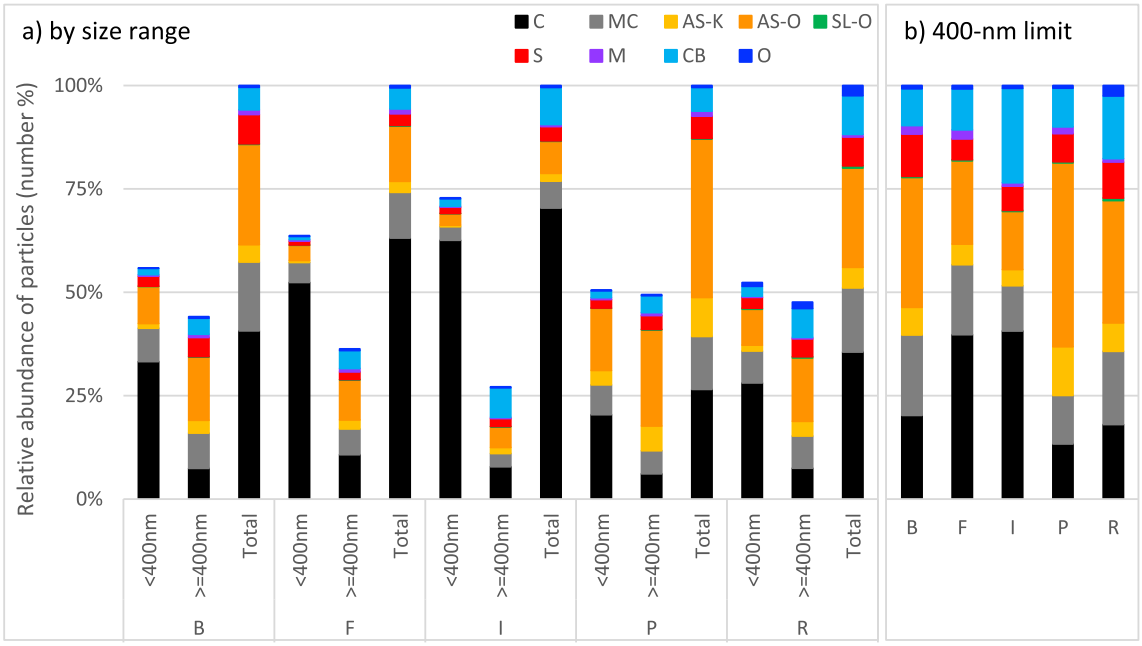

Fig. 5. Average relative abundance of particles (number %) in each mineralogy class across all mines by sampling location. (C = carbonaceous, MC = mixed carbonaceous, ASK = kaolinite-like aluminosilicates, ASO = other aluminosilicates, SLO = other silicates, S = silica, M = heavy minerals, CB = carbonates, O = other; B = roof bolter, F = feeder breaker, I = intake, P = production, R = return.) In a), results are shown for the <400 nm and ≥ 400 nm size ranges, as well as for the total range covered by the SEM analysis. Since the number of samples from each location varied by mine, sample results were first averaged by location in each mine and then by mine, yielding $n = 22$ for the B, F and P locations and $n = 23$ for the I and R locations. In b), results only for the ≥400 nm size range are normalized to compare dust constituents with minimal influence of DPM. Data were computed using number percentage of particles in each mineralogy class.

Table 6
Summary of statistics for comparison of mean particle abundance (number %) in each mineralogy class between sampling locations across all mines. (C = carbonaceous, MC = mixed carbonaceous, ASK = kaolinite-like aluminosilicates, ASO = other aluminosilicates, SLO = other silicates, S = silica, M = heavy minerals, CB = carbonates, O = other; B = roof bolter, F = feeder breaker, I = intake, P = production, R = return.) Analysis excludes P samples from Mines 10, 11, 14, 20, 21, 22.

Class[a]	Mean %					Tukey-Kramer HSD pairs with significant difference (pair *p*-value)				
	B (n = 22)	F (n = 22)	I (n = 23)	P (*n* = 16)	R (n = 23)					
C	20	40	41	18	18	I-R (0.0017)	I-P (0.0067)	F-R (0.0033)	I-B (0.0069)	F-B (0.0123)
MC	19	17	11	16	18	B-I (0.0489)				
ASK	7	5	4	12	7					
ASO	31	20	14	30	30	B-I (0.0112)	P-I (0.0380)	R-I (0.0392)		
SLO	0.3	0.3	0.2	0.4	0.6					
S	10	5	6	8	9					
M	2	2	0.8	2	0.8					
CB	9	10	23	13	15	I-B (0.0337)				
O	0.8	0.8	0.7	0.8	3					

[a] Due to non-normal distributions, data in the following classes was transformed using the cube root: ASK, ASO, SLO, S, M, CB, O.

were excluded from the dataset for statistical analysis, so the results presented in the table can be considered conservative.) They largely confirm the trends discussed above – e.g., the I and F locations have higher abundance of C than B, R and/or P; and the B, P, and R locations have higher ASO than I.

3.3.2. *Effect of mine region and mining method*

Fig. 6 shows the relative abundance (number %) of particles in each mineralogy class when data are simply separated by region (i.e., in or outside of central Appalachia). The overall distribution of particles in the <400 nm size range is relatively similar between the two regional groups (Fig. 6a). However, when only the ≥400 nm particles are considered to minimize the influence of DPM, differences in the mineral dust content are apparent. In the central Appalachian samples, the mineral dust is dominated by AS (ASO + ASK) and it generally contains more S and less CB than the mineral dust in samples from outside of central Appalachia. These differences are likely related to the tendency to cut more rock along with the coal in central Appalachia—and to the bias toward larger mines outside of central Appalachia (i.e., in terms of annual production and mining height), which not only cut less rock but were generally also observed to apply more rock dust in their operations.

While Fig. 6b shows that the abundance of mineral content likely generated from rock strata (ASK + ASO + S) is higher across all sampling locations in central Appalachia, such content is also considerable in the samples from mines located outside of this region—especially in light of the relatively small amount of rock being cut in most of those mines (Table 1). For context, a rough comparison can be made based on the relative rock and coal strata heights being mined and the composition of

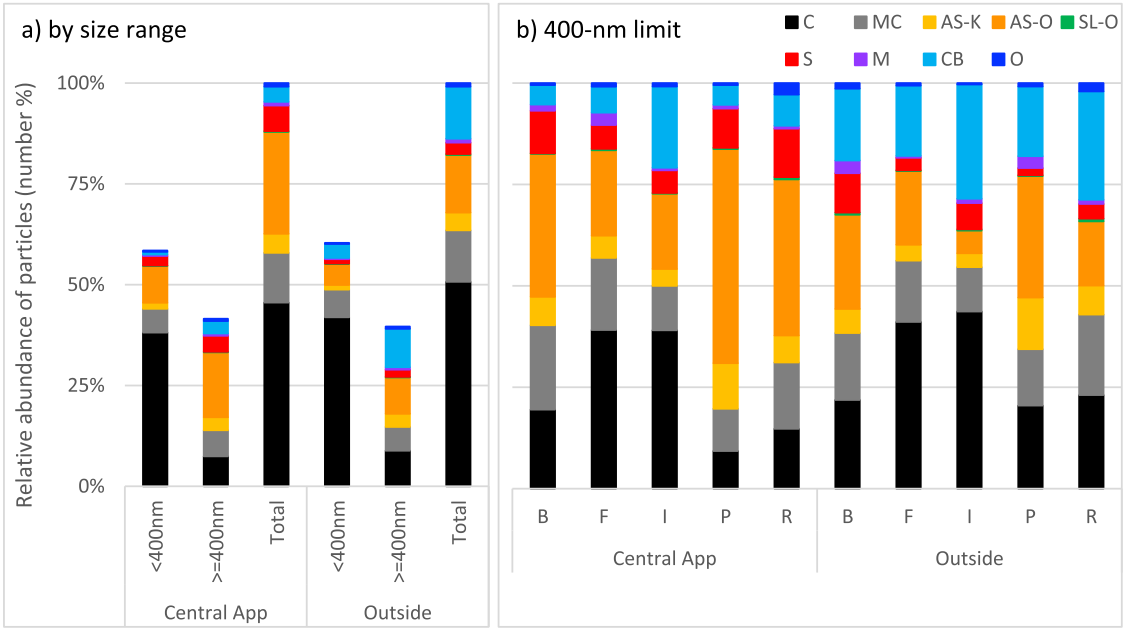

Fig. 6. Average relative abundance of particles (number %) in each mineralogy class for mines in and outside of the central Appalachian region. (C = carbonaceous, MC = mixed carbonaceous, ASK = kaolinite-like aluminosilicates, ASO = other aluminosilicates, SLO = other silicates, S = silica, M = heavy minerals, CB = carbonates, O = other; B = roof bolter, F = feeder breaker, I = intake, P = production, R = return.) In a), results are averaged across all sampling locations for the <400 nm and ≥ 400 nm size ranges, as well as for the total range covered by the SEM analysis. Since the number of samples from each location varied by mine, sample results were first averaged by location in each mine and then across the region, yielding $n = 73$ for central Appalachia and $n = 39$ for outside central Appalachia. In b), results only for the ≥400 nm size range are normalized and separated by sampling location ($n = 15$ for B, F, and I, and $n = 14$ for P and R locations in central Appalachia; n = 7 for B and F, $n = 8$ for I and P, and $n = 9$ for R in mines outside central Appalachia). Data were computed using number percentage of particles in each mineralogy class.

dust in the P samples, which are expected to be dominated by dust generated at the mine face (i.e., rather than influenced by rock dusting, roof bolting or other activities). Rock represents about 37% of the total mining height in the central Appalachian mines, and about 16% in the other mines. However, even excluding the six P samples with exceedingly low C + MC content mentioned above, mineral dust likely sourced from the rock strata (ASO + ASK + S) represents a disproportionately high fraction of the total strata-sourced dust (ASO + ASK+S + C + MC). Using the data shown in Table S2 (and excluding results from Mines 10, 11, 14, 20, 21, 22), the rock-strata sourced dust is about 67% (by number) of the total strata-sourced dust in P samples from central Appalachia, and 49% in P samples from other mines.

Results analogous to those presented in Fig. 6 are presented in Fig. S1 to show differences in mineralogy distributions with respect to the mining method (i.e., continuous miner versus longwall). These results are generally similar to the regional results since most of the longwall mines (5 of 6) are located outside of central Appalachia—though some differences can be observed. For example, similar to the comparison between central Appalachian and outside mines, dust from continuous miner operations appears to have more AS and less CB content than dust from longwall operations, but the differences are exaggerated when comparing mining methods. MC content also appears to be higher in the samples from continuous miner operations than those from longwall operations. This might be related to a greater tendency for coal particles to fall into the MC (rather than C) class when dust also contains more rock-strata sourced dust.

The ANOVA results comparing abundance (number %) of dust particles (≥400 nm) in each mineralogy class by region or mining method are presented in Table 7. These results essentially compare the data shown in Fig. 6b and Fig. S1b. (Note that, again, the six P samples mentioned above were excluded from the dataset for statistical analysis, so the results presented in the table can be considered conservative.) The only significant differences detected for the C and MC classes were between longwall and continuous miner operations, with the former having more C in the P location and the latter having more MC in the B location. The abundance of major mineral components associated with the rock strata (ASO and S) are different for the I, P and/or R samples, with dust from central Appalachian mines or continuous miner operations containing more of these constituents than dust from the outside mines or longwall operations. Regarding CB, samples from central Appalachian mines have lower abundance than those from outside mines the I and R locations; comparing between the mining methods, the continuous miner operations had lower abundance than longwall operations for the F and R locations.

3.4. Particle distributions on the basis of mass

An obvious advantage of SEM-EDX analysis for respirable dust is that it yields particle-level results, thereby allowing determination of size and inferred mineralogy distributions. In the sections above, results have been presented on the basis of particle counts (number %) which are of increasing interest for exposure-response assessments (e.g., Shekarian et al., 2021). Presentation of results on the basis of mass can also be useful—both to illustrate the relationship between particle counts and mass, and to enable comparisons to other analytical methods. As outlined earlier, the SEM-EDX particle size and mineralogy class data was used to estimate particle masses. For samples from all mines included in this study, Tables S3 and S4 summarize the resulting mineralogy distributions (mass %) for the entire size range of particles analyzed and following application of the 400-nm size limit, respectively.

Fig. 7 shows the particle size distributions (mass %) for each mineralogy class both with and without the 400-nm size limit applied to the data. Not surprisingly, exclusion of the finest particles from the dataset has very little impact on the results (i.e., Fig. 7a and b are similar) since those particles contribute relatively little to the dust mass.

Table 7
Summary of statistics for comparison of mean particle abundance (number %) in each mineralogy class between sampling locations by mine region and mining method. Shaded *p*-values indicate significant differences. (C = carbonaceous, MC = mixed carbonaceous, ASK = kaolinite-like aluminosilicates, ASO = other aluminosilicates, SLO = other silicates, S = silica, M = heavy minerals, CB = carbonates, O = other; CA = central Appalachia, OA = outside of central Appalachia; CM = continuous miner, LW = longwall.) Analysis excludes P samples from Mines 10, 11, 14, 20, 21, 22.

		Bolter				Feeder				Intake				Production				Return			
Class[1]		CA	OA	CM	LW	CA	OA	CM	LW	CA	OA	CM	LW	CA	OA	CM	LW	CA	OA	CM	LW
C	Mean (%)	19	22	21	15	39	41	38	49	39	44	42	38	14	23	15	27	15	23	17	20
	p-value	0.7731		0.5461		0.8614		0.3957		0.6669		0.7199		0.2644		0.0161		0.2091		0.6887	
MC	Mean (%)	21	16	22	7.5	18	15	18	12	11	11	11	10	16	16	17	11	16	20	21	8.9
	p-value	0.3909		0.0098		0.5030		0.1939		0.9931		0.8731		0.9937		0.2809		0.5507		0.0571	
ASK	Mean (%)	7.0	6.0	6.6	7.3	5.4	3.9	5.6	2.1	4.2	3.4	4.0	3.6	9.7	14	10	16	6.7	7.1	6.8	7.1
	p-value	0.3239		0.7604		0.3150		0.0576		0.4786		0.6081		0.7248		0.8727		0.4235		0.3605	
ASO	Mean (%)	35	23	32	28	21	18	23	6.0	19	5.6	16	7.4	36	21	35	13	38	16	36	12
	p-value	0.1578		0.3084		0.4056		0.0606		0.0429		0.3490		0.0515		0.0083		0.0247		0.0323	
SLO	Mean (%)	0.1	0.5	0.1	0.9	0.3	0.2	0.3	0.3	0.2	0.3	0.1	0.5	0.5	0.3	0.5	0.2	0.6	0.7	0.3	1.4
	p-value	0.3693		0.0207		0.5440		0.3754		0.6565		0.1420		0.3874		0.2746		0.5782		0.0327	
S	Mean (%)	10	9.6	10	11	5.9	3.1	5.5	2.4	5.6	6.5	5.7	6.5	13	1.8	10	1.4	12	3.6	11	3.0
	p-value	0.7762		0.7203		0.0723		0.1489		0.9246		0.7601		0.0161		0.0592		0.0571		0.0544	
M	Mean (%)	1.5	3.1	1.6	4.1	3.1	0.4	2.6	0.6	0.7	1.1	0.6	1.3	1.4	3.3	2.7	1.0	0.7	1.0	1.0	0.4
	p-value	0.2934		0.7777		0.0071		0.1502		0.1879		0.1233		0.5619		0.8661		0.7479		0.5371	
CB	Mean (%)	4.8	18	5.3	25	6.4	17	6.1	27	20	28	20	32	7.6	19	7.2	29	7.7	27	6.8	39
	p-value	0.0238		0.0787		0.0776		0.0043		0.2704		0.2142		0.2569		0.1207		0.0130		0.0005	
O	Mean (%)	0.5	1.4	0.7	1.2	0.9	0.6	0.8	0.9	0.8	0.3	0.7	0.5	0.8	0.8	0.8	0.8	2.8	2.0	0.6	8
	p-value	0.0511		0.8308		0.6782		0.9236		0.9394		0.7509		0.9491		0.5050		0.4300		0.0016	

[1]*Due to non-normal distributions, data in the following classes was transformed using the cube root: ASK, ASO, SLO, S, M, CB, O*

Comparing Fig. 7 to the same distribution plots in Fig. 3, the difference between particles counts and mass becomes clear. Across all classes, just 2–12% of the dust mass is finer than 1000 nm PAD (regardless of whether or not the 400-nm limit is applied). However, about 25–75% of the particle counts are finer than this size when the 400-nm limit is applied (Fig. 3a); and if all particles are considered (including significant DPM in some samples), about 35–95% of the counts are finer than 1000 nm PAD (Fig. 3b).

Fig. 8 presents the mass-based mineralogy distribution of dust particles (i.e., using the 400-nm size threshold) across the various sampling locations. The abundance of C and MC particles (i.e., likely coal) is remarkably lower than the number-based data in Figs. 5 and 6, which is due to the fact that these particles tend to be relatively fine (see Fig. 3) and are assumed to have relatively low specific gravities (Table 2). On the other hand, the mass-based distributions show even higher mineral abundances than the number-based data since these particles tend to be coarser and are assumed to have higher specific gravities. Nevertheless, the general trends in mineralogy distribution by sampling location are fairly consistent. For example, the mass-based analysis still shows the F location has higher C + MC content than other locations; the I location has higher CB content (i.e., attributed to rock dust product application); and the B, P and R locations have higher mineral content associated with the rock strata (ASK+ASO + S). And, again, the rock-strata sourced dust is even more abundant in the samples from central Appalachian mines, whereas the coal and rock-dust-product sourced dust are more abundant in samples from the other mines. The relatively higher silica content in the central Appalachian samples, specifically, fits with dust monitoring data collected for regulatory compliance; that data includes the quartz mass content in respirable coal mine dust, which is consistently higher in central Appalachian mines than mines in other regions (Doney et al., 2019).

3.5. Implications for dust control, mine monitoring, and occupational health outcomes

The results presented herein have implications for dust control and monitoring activities. By elucidating the primary constituents of respirable coal mine dust, important insights can be gained regarding primary dust sources. Consistent with findings in the earlier study of Mines 1–8 (Sarver et al., 2019a), across this much larger, 25-mine dataset, results indicate three primary dust sources: rock strata, including high-silica strata; rock-dusting products; and coal strata. Additionally, diesel emissions (where present) can contribute significant numbers of respirable particles. It is important to reiterate that the data presented here should be viewed as complementary to that collected by routine monitoring programs in coal mines (e.g., for regulatory compliance). Whereas the latter yields total mass concentration of respirable dust (mg/m^3), the current data enable understanding of the major mineralogic components and particle sizes that makeup the dust.

Dust control and monitoring efforts have long been targeted toward

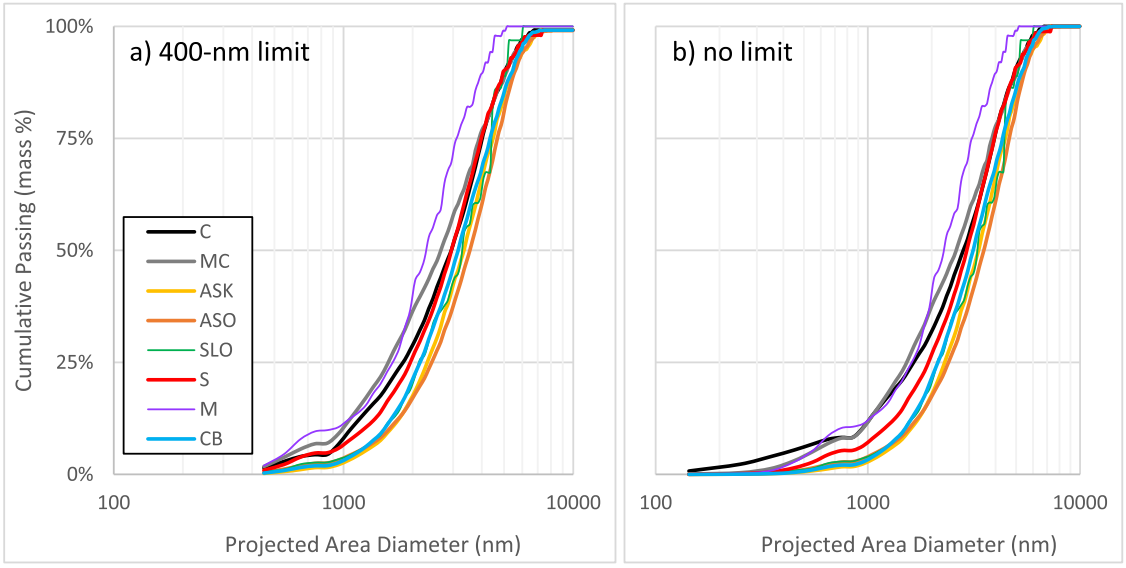

Fig. 7. Average cumulative particle size distributions (mass %) across all mines and sampling locations by mineralogy class (C = carbonaceous, MC = mixed carbonaceous, ASK = kaolinite-like aluminosilicates, ASO = other aluminosilicates, SLO = other silicates, S = silica, M = heavy minerals, CB = carbonates, O = other). Results are shown a) with and b) without the 400-nm threshold established to minimize the influence of DPM on the C class; $n = 112$ for both plots. Data were computed using estimated mass percentage of particles in 100-nm wide size bins, with points plotted at the bin mid-size.

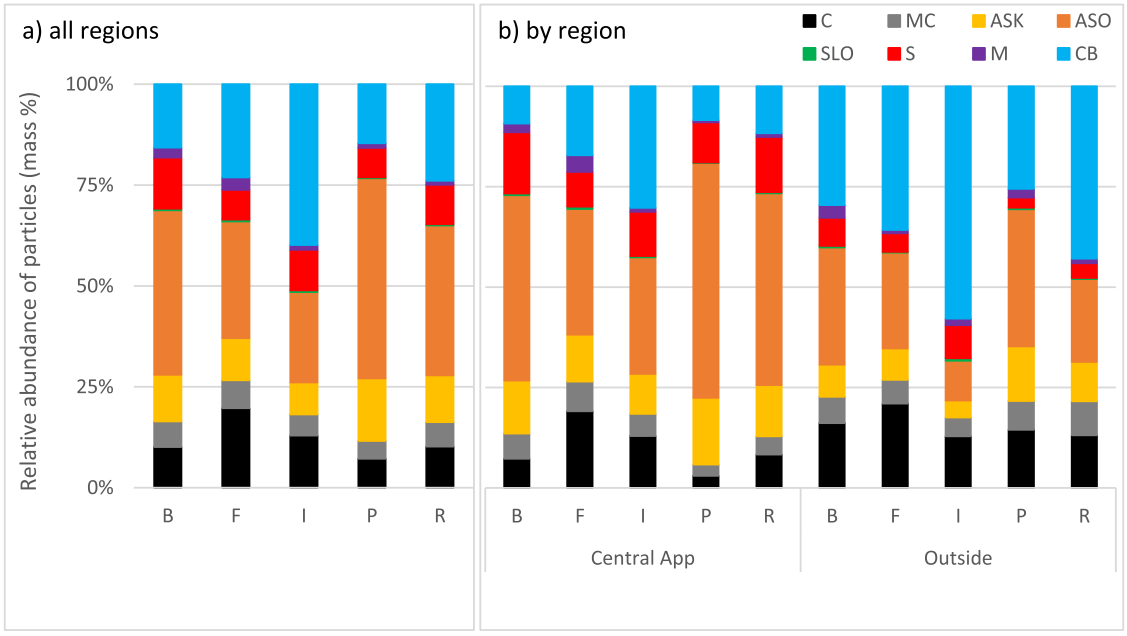

Fig. 8. Average relative abundance of particles (mass %) in each mineralogy class by sampling location. (C = carbonaceous, MC = mixed carbonaceous, ASK = kaolinite-like aluminosilicates, ASO = other aluminosilicates, SLO = other silicates, S = silica, M = heavy minerals, CB = carbonates, O = other; B = roof bolter, F = feeder breaker, I = intake, P = production, R = return.) In a), results are shown across all mine (n values same as in Fig. 5). In b), results are separated by mine region (n values same as in Fig. 6. Data were computed using mass percentage of particles ≥400 nm in each mineralogy class.

the production face and roof bolting activities where the mass concentration of respirable dust is relatively high (Goodman and Organiscak, 2002; Goodman et al., 2006; Colinet et al., 2010; National Academies, 2018). The results presented here reinforce those priorities, since dust in these (and downwind) areas also tends to have high abundance of rock-strata sourced particles including silica, which is generally considered the most hazardous constituent in respirable coal mine dust (Colinet et al., 2010; Reynolds et al., 2018). Indeed, the contribution of dust from the rock-strata appears to be inordinately high (on both a mass and number-basis) near the production face in many mines. This observation begs for further work to explore the responsible factors. As mentioned above, one possibility is that typical dust controls such as water sprays or scrubbers are more efficient for coal than for mineral particles.

The influence of rock dusting practices on respirable dust in coal mines has also been a point of interest in recent years as mines have increased their application of rock dust products to improve safety (National Academies, 2018). The results presented here clearly demonstrate that rock dusting activities can contribute to the respirable dust fraction. Though common products (i.e., high purity limestone powders) are generally considered to present minimal health risks (e.g.,

Khaliullin et al., 2019), knowledge of their relative abundance in respirable dust is still important for assessing and responding to overall exposure risks. For example, knowledge that the respirable dust in a given area is both consistently low in mass concentration and largely associated rock dusting activities might allow monitoring resources to be prioritized for other areas (i.e., with more variable or consistently concerning dust concentrations and/or constituents).

In addition to informing dust control and monitoring strategies, the current results may shed light on recent disease trends. While total mass concentrations of respirable dust generally appear to have been declining across all regions of the United States for decades (Doney et al., 2019), the characteristics of the dust including mineralogic constituents and relative particle sizes could have shifted to become more hazardous (National Academies, 2018). For instance, given equal mass exposures, dust with increased relative abundance of rock-strata sourced particles and/or finer particles might cause a more severe lung response than dust with higher relative abundance of coal and/or coarser particles. Particle size has been the focus of several studies on respirable dust toxicity (Mischler et al., 2016), and there has been limited work on specific dust constituents such as crystalline silica and pyrite (Castranova et al., 1997; Cohn et al., 2006). However, the results presented here may serve as a jumping off point for studies on the relative and combined effects of the group of primary constituents identified in most dust samples (i.e., silicates, silica, coal, carbonates, DPM).

4. Conclusions

SEM-EDX analysis of respirable coal mine dust can offer new insights on characteristics such as particle size and mineralogy, which may be critical to understanding dust sources—as well as exposure risks and outcomes. In this study, respirable dust samples were collected and analyzed from 25 underground coal mines in the United States. Since sample collection and analysis procedures were identical across all mines, the dataset provides a unique opportunity for direct comparison of dust characteristics across a large number of operations.

Particle size analysis showed that dust was frequently in the submicron range, including silica, silicates and diesel particulates. Though these very fine particles contribute relatively little to the total dust mass—which is the focus of routine dust monitoring measurements—they may play an outsized role in the context of lung response. As such, an understanding of particle size distributions is important, including how they vary with different dust sources and controls. Here, results indicated that dust particle sizes (excluding diesel particulates) tended to be finest in areas nearby active dust generation from the mine strata (i.e., downwind from the production face, roof bolting or in the return).

Analysis of mineralogy distributions confirmed key trends in dust sources with respect to specific sampling locations, mine region, and mining method. In intake airways, dust tends to show more influence from rock dust application; in mines operating diesel equipment, the emissions are most noticeable in the intake also (i.e., where other dust sources are minimal). On the other hand, in locations nearby to production and roof bolting activities, dust is clearly sourced from the mine strata. Just downwind from the production face, the ratio of dust apparently sourced from the rock versus coal strata appears inordinately high; this trend was previously noted for some of the mines studied here (Sarver et al., 2019a), and the expanded dataset in the current study indicates it is pervasive across regions and mining methods. Still, rock-strata sourced dust is generally more abundant in samples from central Appalachian or continuous miner operations than in samples from other regions or longwall operations. This finding is attributed to the tendency to mine thinner coal seams and more rock in central Appalachian or continuous miner operations.

Declaration of Competing Interest

Author states that there is not any conflict of interest.

Acknowledgements

The authors gratefully acknowledge the Alpha Foundation for the Improvement of Mine Safety and Health and the National Institute for Occupational Safety and Health for funding this work. We would like to thank our many industry partners for their interest in this research, support with mine access and logistical assistance with dust sampling. Many thanks also to Rachel Sellaro Calvert, Meredith Scaggs Witte, Victoria Johann Essex, Alex Norris, Kyle Louk, Eleftheria Agioutanti, Mohammad Rezaee. Jonathan Gonzalez and Lizeth Jaramillofor their assistance with dust sampling and analysis; and to Young Ho Yun and Adeline Guthrie of the Statistical Applications and Innovations Group (SAIG) at Virginia Tech for help with statistical analysis. Views expressed here represent those of the authors and do not imply endorsement by the sponsor or partners.

Appendix A. Supplemental Information

Supplementary data to this article can be found online at https://doi.org/10.1016/j.coal.2021.103851.

References

Abbasi, B., Wang, X., Chow, J.C., Watson, J.G., Peik, B., Nasiri, V., Riemenschnitter, K.B., Elahifard, M., 2021. Review of respirable coal mine dust characterization for mass concentration, size distribution and chemical composition. Minerals 11, 426. https://doi.org/10.3390/min11040426.

Almberg, K.S., Halldin, C.N., Blackley, D.J., Laney, A.S., Storey, E., Rose, C.S., Go, L.H.T., Cohen, R.A., 2018. Progressive massive fibrosis resurgence identified in U.S. coal miners filing for black lung benefits, 1970-2016. Ann. Am. Thorac. Soc. 15 (12), 1420–1426. https://doi.org/10.1513/AnnalsATS.201804-261OC.

Barone, T.L., Patts, J.R., Janisko, S.J., Colinet, J.F., Patts, L.D., Beck, T.W., Mischler, S.E., 2016. Sampling and analysis method for measuring airborne coal dust mass in mixtures with limestone (rock) dust. J. Occup. Environ. Hyg. 13, 284–292. https://doi.org/10.1080/15459624.2015.1116694.

Birch, M.E., Noll, J.D., 2004. Submicrometer elemental carbon as a selective measure of diesel particulate matter in coal mines. J. Environ. Monit. 6 (10), 799–806. https://doi.org/10.1039/b407507b.

Blackley, D.J., Halldin, C.N., Laney, A.S., 2018. Continued increase in prevalence of coal workers' pneumoconiosis in the United States, 1970–2017. Am. J. Public Health 180 (9), e1–e3. https://doi.org/10.2105/AJPH.2018.304517.

Castranova, V., Vallyathan, V., Ramsey, D., McLaurin, J.L., Pack, D., Leonard, S., Barger, M.W., Ma, J.Y.C., Dalal, N.S., Teass, A., 1997. Augmentation of pulmonary reactions to quartz inhalation by trace amounts of iron-containing particles. Environ. Health Perspect. 105 (Suppl. 5), 1319–1324. https://doi.org/10.1289/ehp.97105s51319.

Code of Federal Regulations, 2021. Title 30, Part 70: Mandatory Health Standards – Underground Coal Mines.

Cohen, R.A., Petsonk, E.L., Rose, C., Young, B., Regier, M., Najmuddin, A., Abraham, J.L., Churg, A., Green, F.H.Y., 2016. Lung pathology in U.S. coal workers with rapidly progressive pneumoconiosis implicates silica and silicates. Am. J. Respir. Crit. Care Med. 193 (6), 673–680. https://doi.org/10.1164/rccm.201505-1014OC.

Cohn, C.A., Laffers, R., Simon, S.R., O'Riordan, T., Schoonen, A.A., 2006. Role of pyrite in formation of hydroxyl radicals in coal: possible implications for human health. Partic. Fibre Toxicol. 3 (16) https://doi.org/10.1186/1743-8977-3-16, 10 pages.

Colinet, J.F., Rider, J.P., Listak, J.M., Organiscak, J.A., Wolfe, A.L., 2010. Best Practice for Dust Control in Coal Mining. Information Circular 9517. DHHS (NIOSH) Publication No. 2010-110 [online]. Available at. https://www.cdc.gov/niosh/mining/userfiles/works/pdfs/2010-110.pdf.

Doney, B.C., Blackley, D., Hale, J.M., Halldin, C., Kurth, L., Syamlal, G., Laney, A.S., 2019. Respirable coal mine dust in underground mines, United States, 1982–2017. Am. J. Ind. Med. 62 (6), 478–485. https://doi.org/10.1002/ajim.22974.

Goodman, G.V.R., Organiscak, J.A., 2002. An Evaluation of Methods for Controlling Silica Dust Exposures on Roof Bolters. SME Preprint 02-163. Society for Mining, Metallurgy, and Exploration, Inc, Littleton, CO.

Goodman, G.V.R., Beck, T.W., Pollock, D.E., Colinet, J.F., Organiscak, J.A., 2006. Emerging technologies control respirable dust exposures for continuous mining and roof bolting personnel. In: Proceedings of the 11th US/North American Mine Ventilation Symposium. Boca Raton, FL, pp. 211–216.

Hall, N.B., Blackley, D.J., Halldin, C.N., Laney, A.S., 2019. Current review of pneumoconiosis among US coal miners. Curr. Environ. Health Rep. 6 (3), 137–147. https://doi.org/10.1007/s40572-019-00237-5.

ISO, 1995. Air Quality–Particle Size Fraction Definitions for Health-Related Sampling. ISO 7708:1995(en). International Organization Standardization, Geneva.

Jelic, T.M., Estalilla, O.C., Sawyer-Kapla, N.P.R., Plata, M.J., Powers, J.T., Emmett, M., Kuenstner, J.T., 2017. Coal mine dust desquamative chronic interstitial pneumonia: a precursor of dust-related diffuse fibrosis and of emphysema. Int. J. Occup. Environ. Med. 8 (3), 153–165. https://doi.org/10.15171/ijoem.2017.1066.

Johann-Essex, V., Keles, C., Rezaee, M., Scaggs-Witte, M., Sarver, E., 2017a. Respirable coal mine dust characteristics in samples collected in central and northern Appalachia. Int. J. Coal Geol. 182, 85–93. https://doi.org/10.1016/j.coal.2017.09.010.

Johann-Essex, V., Keles, C., Sarver, E., 2017b. A computer-controlled SEM-EDX routine for characterizing respirable coal mine dust. Minerals 7 (1), 15. https://doi.org/10.3390/min7010015.

Khaliullin, T.O., Kisin, E.R., Yanamala, N., Guppi, S., Harper, M., Lee, T., Shvedova, A.A., 2019. Comparative cytotoxicity of respirable surface-treated/untreated calcium carbonate rock dust particles in vitro. Toxicol. Appl. Pharmacol. 362, 67–76. https://doi.org/10.1016/j.taap.2018.10.023.

LaBranche, N., Keles, C., Sarver, E., Johnstone, K., Cliff, D., 2021. Characterization of particulates from Australian underground coal mines. Minerals 11 (5), 447. https://doi.org/10.3390/min11050447.

Mischler, S.E., Cauda, E.G., Giuseppe, M.D., McWilliams, L.J., Croix, C.St., Sun, M., Franks, J., Ortiz, L.A., 2016. Differential activation of RAW 264.7 macrophages by size-segregated crystalline silica. J. Occup. Med. Toxicol. 11 (57) https://doi.org/10.1186/s12995-016-0145-2, 15 pages.

MSHA, 2008. Method No. MSHA P7: Infrared Determination of Quartz in Respirable Coal Mine Dust. United States Department of Labor-MSHA-Pittsburgh Safety and Health Technology Center.

National Academies of Sciences, Engineering, and Medicine, 2018. Monitoring and Sampling Approaches to Assess Underground Coal Mine Dust Exposures. The National Academies Press, Washington, DC. https://doi.org/10.17226/25111.

Oberdörster, G., Oberdörster, E., Oberdörster, J., 2005. Nanotoxicology: an emerging discipline evolving from studies of ultrafine particles. Environ. Health Perspect. 113 (7), 823–839. https://doi.org/10.1289/ehp.7339.

Pan, L., Golden, S., Assemi, S., Sime, M.F., Wang, X., Gao, Y., Miller, J., 2021. Characterization of particle size and composition of respirable coal mine dust. Minerals 11 (3), 276. https://doi.org/10.3390/min11030276.

Phillips, K., Keles, C., Scaggs, M., Johann, V., Rezaee, M., Sarver, E., 2017. Considerations for TGA of respirable coal mine dust samples. In: Proceedings of the 16th North American Mine Ventilation Symposium, Golden, Colorado, June 17-22, 7, pp. 1–9.

Phillips, K., Keles, C., Sarver, E., Scaggs-Witte, M., 2018. Coal and mineral mass fractions in personal respirable dust samples collected by central Appalachian miners. Min. Eng. 70 (6), 16–30.

Reynolds, L.E., Blackley, D.J., Colinet, J.F., Potts, J.D., Storey, E., Short, C., Carson, R., Clark, K.A., Laney, A.S., Halldin, C.N., 2018. Work practices and respiratory health status of Appalachian coal miners with progressive massive fibrosis. J. Occup. Environ. Med. 60 (11), e575–e581. https://doi.org/10.1097/JOM.0000000000001443.

Riediker, M., Zink, D., Kreyling, W., Oberdörster, G., Elder, A., Graham, U., Lynch, I., Duschl, A., Ichihara, G., et al., 2019. Particle toxicology and health - where are we? Partic. Fibre Toxicol. 16 (19), 33. https://doi.org/10.1186/s12989-019-0302-8.

Sarver, E., Keles, C., Rezaee, M., 2019a. Beyond conventional metrics: Comprehensive characterization of respirable coal mine dust. Int. J. Coal Geol. 207, 84–95. https://doi.org/10.1016/j.coal.2019.03.015.

Sarver, E., Keles, C., Rezaee, M., 2019b. Characteristics of respirable dust in eight Appalachian coal mines: a dataset including particle size and mineralogy distributions, and metal and trace element mass concentrations. Data Brief 25, 104032. https://doi.org/10.1016/j.dib.2019.104032.

Scheepers, P.T.J., Micka, V., Muzyka, V., Anzion, R., Dahmann, D., Poole, J., Bos, R.P., 2003. Exposure to dust and particle-associated 1-nitropyrene of drivers of diesel-powered equipment in underground mining. Ann. Occup. Hyg. 47 (5), 379–388. https://doi.org/10.1093/annhyg/meg036.

Shekarian, Y., Rahimi, E., Rezaee, Su, Roghanchi, P., 2021. Respirable coal mine dust: a review of respiratory deposition, regulations, and characterization. Minerals 11 (696), 25. https://doi.org/10.3390/min11070696.

Su, X., Ding, R., Zhuang, X., 2020. Characteristics of Dust in Coal Mines in Central North China and its Research significance. ACS Omega 5 (16), 9233–9250. https://doi.org/10.1021/acsomega.0c00078.

Trechera, P., Moreno, P., Moreno, N., Zhuang, X., Li, B., Li, J., Shangguan, Y., Kandler, K., Dominguez, A., Kelly, F., Querol, X., 2020. Mineralogy, geochemistry and toxicity of size-segregated respirable deposited dust in underground coal mines. J. Haz. Mater. 399 https://doi.org/10.1016/j.jhazmat.2020.122935.

Zhang, R., Liu, S., Zheng, S., 2021. Characterization of nano-to-micron sized respirable coal dust: Particle surface alteration and the health impact. J. Haz. Mater. 413 https://doi.org/10.1016/j.jhazmat.2021.125447.